ELECTRO-OPTICAL DEVICES

Electro-optic (EO) devices control light by using an electric field to induce changes in the refractive index and/or absorption of the material.

The phenomena related to refractive index changes are known generally as the EO effect. When the induced change in the refractive index is proportional to the applied electric field *E*, this is known as the linear EO effect or the Pockels effect. When the induced change in the refractive index is proportional to E^2, this is called the quadratic EO effect or the Kerr effect. The former case occurs only in piezoelectric crystals that do not have point symmetry, whereas the latter occurs in all crystals. The most advanced material showing a large Pockels effect is $LiNbO_3$ (lithium niobate: LN) crystal. Because the EO effect does not depend on the frequency of the drive voltage excluding the influence of the piezoelectric effect, various LN devices such as optical modulators, switches, and directional couplers are being developed for practical use in optical fiber communication, signal processing, and sensing technologies.

The typical phenomena associated with electrically induced absorption change in semiconductors are known generally as the Stark effect and the Franz–Keldysh effect. In the Stark effect, atoms placed in an electrostatic field cause band edge shift. The phenomenon known as the quantum-confined Stark effect (QCSE), wherein an electric field applied vertically to a semiconductor quantum well induces a shift in the absorption spectra of excitons in the well, is also included under the term of the Stark effect. Well-known devices using the QCSE include electroabsorption modulators and self-electro-optic-effect devices (SEED). The Franz–Keldysh effect is a phenomenon in which the density of states at the edge of a valence band and conduction band in the semiconductor changes because of an applied electric field, causing the fundamental absorption edge to shift to the long wavelength side and the absorption in that vicinity to increase. This is also known as the electroabsorption effect, and it is often employed in high-speed optical modulators using compound semiconductors. The absorption change is related to the refractive index change by the Kramers–Kronig relation, so semiconductor waveguide devices using the QCSE and Franz–Keldysh effect can control the optical phase of the guided beam.

There are also semiconductor devices that control light by means of carrier injection and depletion, which change the refractive index and absorption. Other phenomena employed in semiconductor devices include the free carrier plasma effect and the band-filling effect.

Acoustooptic devices, which diffract light by periodically changing the refractive index generated by acoustic waves and liquid crystal devices, in which the alignment of liquid crystal molecules is controlled by an ac electric field, are also electro-optical devices with functions similar to EO devices, but these will not be discussed here. Interested readers may refer to Refs. 1 and 2 for further information.

In the 1960s, when the laser was invented, EO crystals such as potassium dihydrogen phospher (KH_2PO_4), barium titanate ($BaTiO_3$), LN, and lithium tantalate ($LiTaO_3$) attracted a great deal of attention as new materials for optical devices. Research focused primarily on crossed-Nicol-type optical modulators that controlled the retardation, a phase difference between two linearly polarized light components. It was expected that these EO modulators would be applied in early optical communications, but unfortunately they had many problems including (1) the need for a high applied voltage, (2) very large size, and (3) difficulty for broadband modulation. To solve these problems, Miller proposed the optical integrated circuit in 1969 (3). In 1974, Schmit and Kaminow were the first to create a thin-film optical waveguide on an LN crystal with low insertion loss (4). Ever since, the development of LN waveguide devices using the Pockels effect has been pursued aggressively, resulting in the development of all manner of devices including optical modulators with low drive voltage, directional couplers, optical switches, and even optical integrated circuits combining all of these on a single chip. This progress briefly faltered in the 1980s because of the dramatic developments in semiconductor lasers. These, however, have had problems with frequency chirping during high-speed pulse modulation, so interest has once again turned to super high-speed optical control by LN waveguide modulators as a key technology for realizing ultra-high-speed communication.

EO devices using III-V compound semiconductors such as GaAs, AlGaAs, InP, InGaAs, and GaInAsP have a smaller EO effect than the LN crystal, so their performance was greatly inferior to that of LN waveguide devices until the 1980s. Advances, however, in the fabrication technique for super lattice structures, then made it possible to fabricate good waveguide devices that employ distinctive physical phenomena such as the QCSE, the Franz–Keldysh effect, and band filling. The performance of these devices now stands comparison with that of LN devices. Furthermore, because two-dimensional EO devices and the monolithic integration of photoemitters, photodetectors, optical amplifiers, and drive circuits are possible with the waveguide devices using semiconductors, it is expected that their importance will increase in the future.

EO EFFECT

When the coordinates of piezoelectric crystals are x, y, and z, and the principal refractive indices in the direction of those coordinates are n_x, n_y, and n_z, respectively, the index ellipsoid representing the optical properties of the crystals can be given as

$$x^2/n_x^2 + y^2/n_y^2 + z^2/n_z^2 = 1 \tag{1}$$

If $n_x = n_y = n_z$, they are cubic crystals including $\bar{4}3$m and 23 classes. When $n_x = n_y \neq n_z$, they are uniaxial crystals including 3m, 42m and so on, and if $n_x \neq n_y \neq n_z$, they are biaxial crystals. If the optical axis of the uniaxial crystals is along the z axis, $n_x = n_y = n_o$ is an ordinary refractive index, and $n_z = n_e$ is an extraordinary refractive index.

Applying an electric field to these crystals induces refractive index changes due to the EO effect. The index ellipsoid can be expressed as

$$[1/n_x^2 + \Delta_{xx}]x^2 + [1/n_y^2 + \Delta_{yy}]y^2 + [1/n_z^2 + \Delta_{zz}]z^2 + 2\Delta_{yz}yz + 2\Delta_{zx}zx + 2\Delta_{xy}xy = 1 \tag{2}$$

where Δ_{ij} is the amount of change in a coefficient of the ij part of the index ellipsoid caused by the electric field. Because the Pockels effect is generally larger than the Kerr effect, here we focus only on the influence of the Pockels effect. Δ_{ij} caused by the Pockels effect can be expressed by the following determinant:

$$\begin{vmatrix} \Delta_{xx} \\ \Delta_{yy} \\ \Delta_{zz} \\ \Delta_{yz} \\ \Delta_{zx} \\ \Delta_{xy} \end{vmatrix} = \begin{vmatrix} r_{11} & r_{12} & r_{13} \\ r_{21} & r_{22} & r_{23} \\ r_{31} & r_{32} & r_{33} \\ r_{41} & r_{42} & r_{43} \\ r_{51} & r_{52} & r_{53} \\ r_{61} & r_{62} & r_{63} \end{vmatrix} \begin{vmatrix} E_x \\ E_y \\ E_z \end{vmatrix} \tag{3}$$

where E_x, E_y, and E_z are the electrical fields applied in the directions of the x, y, and z axes, respectively.

r_{ij} is the third-rank tensor known as the linear EO coefficient, and because of the symmetry of the crystals, a number of coefficients are equal or 0. For example, in class 3m, which includes ferroelectric crystals such as LN and $LiTaO_3$, often used in optical waveguide devices, all coefficients except for $-r_{12} = r_{22} = -r_{61}$, $r_{13} = r_{23}$, r_{33}, and $r_{42} = r_{51}$ are zero. In classes $\bar{4}3$m, to which belong semiconductor crystals with high symmetry such as GaAs, GaP, ZnS, and CdTe, all coefficients except for $r_{41} = r_{52} = r_{63}$ are zero.

The value of the EO coefficient r_{ij} differs between the clamped state in which constant strain arises in the crystals and the free state in which constant stress is applied to the crystals. The former is known as the intrinsic EO coefficient and is represented by r_{ij}^{S}. The latter includes an effect by which the refractive index changes as a result of crystal deformation by the photoelastic effect, based on the piezoelectric and electrostrictive effects, and can be represented by r_{ij}^{T}. r_{ij}^{T} must be used when designing EO devices that operate at low frequencies.

The following are examples of the properties demanded of EO crystals: (1) a large EO effect; (2) high-transparency with no coloration by impurities; (3) optical homogeneity; (4) large single crystals; and (5) no deliquescence plus optical and me-

Table 1. Electro-optic Material Parameters

Material	Symmetry	r_{ij}^{T}, r_{ij}^{S} (pm/V)	Refractive Index	Wavelength (nm)
GaAs	$\bar{4}3$m	$r_{41}^{T} = 1.6, r_{41}^{S} = 0.94$	$n_o = 3.346$	1900
GaP	$\bar{4}3$m	$r_{41}^{T} = 1.00, r_{41}^{S} = 0.97$	$n_o = 3.31192$	1000
$LiNbO_3$	3m	$r_{33}^{T} = 30.9, r_{33}^{S} = 30.8$	$n_o = 2.2868$	633
		$r_{13}^{T} = 9.6, r_{13}^{S} = 8.6$	$n_o = 2.2030$	633
		$r_{22}^{T} = 6.8, r_{22}^{S} = 3.4$		
		$r_{51}^{T} = 32.6, r_{51}^{S} = 28$		
$LiTaO_3$	3m	$r_{33}^{T} = 30.5, r_{33}^{S} = 35.8$	$n_o = 2.1774$	632.8
		$r_{13}^{T} = 8.4, r_{13}^{S} = 7.9$	$n_e = 2.1818$	632.8
		$r_{22}^{T} = 0.2, r_{22}^{S} = 1$		
		r_{51}^{T},[a] $r_{51}^{S} = 20$		
KH_2PO_4	$\bar{4}2$m	$r_{41}^{T} = 8.6, r_{41}^{S} = 8.6$	$n_o = 1.50737$	632.8
		$r_{63}^{T} = 10.5, r_{63}^{S} = 8.8$	$n_e = 1.46685$	632.8
$BaTiO_3$	4mm	$r_{33}^{T} = 80, r_{33}^{S} = 28$	$n_o = 2.437$	546.1
		$r_{13}^{T} = 24, r_{13}^{S} = 8$	$n_e = 2.365$	546.1
		$r_{51}^{T} = 1280, r_{51}^{S} = 820$		
$Ba_2NaNb_5O_{15}$	2mm	$r_{13}^{T} = 15, r_{13}^{S} = 6.1$	$n_a = 2.3222$	632.8
		$r_{23}^{T} = 13, r_{23}^{S} = 8$	$n_b = 2.3205$	632.8
		$r_{33}^{T} = 48, r_{33}^{S} = 24.3$	$n_c = 2.2177$	632.8
		$r_{42}^{T} = 92, r_{42}^{S} = 79$		

[a] Unknown.

chanical stability. Table 1 shows the properties of EO crystals, which are often used in for EO devices.

Examples

Let's estimate the optical phase changes resulting from the EO effect by taking the class 3m crystal as an example. When we apply an electric field parallel to the z axis of the crystal, Δ_{ij} of Eq. (3) can be expressed as follows:

$$\begin{aligned}\Delta_{xx} &= \Delta_{yy} = r_{13}E_z \\ \Delta_{zz} &= r_{33}E_z \\ \Delta_{yz} &= \Delta_{zx} = \Delta_{xy} = 0\end{aligned} \tag{4}$$

Substituting Eq. (4) for Eq. (2), we obtain

$$(1/n_\mathrm{o}^2 + r_{13}E_z)x^2 + (1/n_\mathrm{o}^2 + r_{13}E_z)y^2 + (1/n_\mathrm{e}^2 + r_{33}E_z)z^2 = 1 \tag{5}$$

using $n_x = n_y = n_\mathrm{o}$, $n_z = n_\mathrm{e}$ because the crystal is uniaxial.

Equation (5) represents the index ellipsoid where all cross products are eliminated. Accordingly, there is no rotation of principal axes and only the refractive indices change. The refractive indices caused by the EO effect can be calculated from Eq. (5)

$$\begin{aligned}n_x &= n_y = n_\mathrm{o} - n_\mathrm{o}^3 r_{13}E_z/2 \\ n_z &= n_\mathrm{e} - n_\mathrm{e}^3 r_{33}E_z/2\end{aligned} \tag{6}$$

where we use the relations $r_{13}E_z \ll 1/n_\mathrm{o}^2$, $r_{33}E_z \ll 1/n_\mathrm{e}^2$.

See Ref. 5 for the relationship between the direction of an applied electric field, the principal axes, and refractive indices for various configurations of the crystallographic group often used in EO devices.

ELECTRO-OPTIC MODULATORS USING BULK CRYSTALS

Let's take the example of an EO modulator using a bulk crystal in point group 3m for understanding the outline of EO devices. Most bulk EO modulators are crossed-Nicol type modulators, which control the retardation. This type of EO modulator can easily modulate the intensity of a light beam incident to the EO crystal, but the output light intensity depends strongly on the temperature because of natural birefringence. In order to eliminate for use in a wide range of temperatures, an optical modulator that compensates natural birefringence was invented in which a half-wave plate is inserted between two EO crystals of the same size, as shown in Fig. 1. Linearly polarized light propagates along the y axis of the crystal, and its electric vector crosses the x and z axes of the crystal at 45°. This incident beam is decomposed into two components polarized in the x and z directions with equal amplitude within the EO crystal. Both components sense different refractive indices and index changes induced by the EO effect. The light component polarized in the x axis propagates along the y axis and senses a refractive index of $n_\mathrm{o} - n_\mathrm{o}^3 r_{13}E/2$ in the incident side crystal, but because the plane of polarization rotates 90° through the half-wave plate, the light component senses a refractive index of $n_\mathrm{e} + n_\mathrm{e}^3 r_{33}E/2$ within the output side crystal. The other light component, polarized

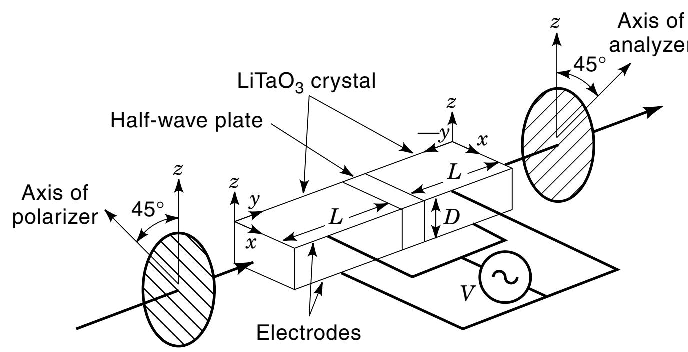

Figure 1. Configuration of electrooptic light modulator consisting of two bulk EO crystals of the same size and a half-wave plate. This device modulates incident light while compensating natural birefringence.

in the z axis, senses a refractive index of $n_\mathrm{e} - n_\mathrm{e}^3 r_{33}E/2$ within the input side crystal, and a refractive index of $n_\mathrm{o} - n_\mathrm{o}^3 r_{13}E/2$ within the output side crystal. The retardation Θ between these two light components is therefore given by

$$\Theta = 2\pi LV(n_\mathrm{e}^3 r_{33} - n_\mathrm{o}^3 r_{13})/D\lambda \tag{7}$$

where L and D are, respectively, the length and depth of the EO crystal and λ is the wavelength of light.

The configuration shown in Fig. 1 is the so-called crossed-Nicol state where both axes of the polarizer and analyzer cross each other at 90°. Normalized output power I is given by

$$I = \sin^2(\Theta/2) \tag{8}$$

The applied voltage corresponding to $\Theta = \pi$ is known as the half-wave voltage V_π. It is one of the important parameters characterizing device performance. Other important performance parameters include the extinction ratio and frequency bandwidth. The extinction ratio is represented by the ratio of the maximum and minimum values of the output power of the actual modulator engaged in the static retardation, based on such factors as crystal nonhomogeneity and fabrication error.

In order to obtain a low V_π, D/L must be lowered as far as possible. Because bulk crystal devices do not have a waveguide structure, however, the ratio is naturally limited by the thickness and length of the device. When introducing safety factor S, representing the ease of propagation of a beam within bulk crystals, the following relationship between depth D and length $2L$ of the bulk crystals should hold (6)

$$D = 2\sqrt{2}S(\lambda L/n\pi)^{1/2} \tag{9}$$

$S \geqq 6$ is the state in which incident beam loss is low and alignment is easy. Let's estimate V_π of the bulk EO modulator shown in Fig. 1 by the following parameters: (1) $LiTaO_3$ crystal, (2) $L = 10$ mm, (3) $\lambda = 0.633$ nm, and (4) $S = 6$. Substituting these values and refractive indices and the EO coefficients in Table 1 into Eqs. (7)–(9), we obtain $V_\pi \fallingdotseq 59$ V, which is fairly large.

A 1 × 2 (1 input for 2 outputs) optical switch that replaces the analyzer in Fig. 1 with a polarizing beam splitter has been proposed (7). This switch has been demonstrated distributing a baseband TV signal with a high signal to noise ratio (SNR). EO modulators using cubic EO crystals such as $Bi_{12}SiO_{20}$ and $Bi_{12}GeO_{20}$ have also been investigated as electric field sensors. These crystals have a lower EO coefficient than $LiTaO_3$ crystals, but they have been used for high-voltage sensors in the field of high electric power transmission because they exhibit extremely superior temperature properties. Some devices apply an electric field to the z axis of the $Bi_{12}SiO_{20}$ or $Bi_{12}GeO_{20}$ crystal and pass light through the z axis of the crystal. These are known as spatial light modulators, and they can modulate two-dimensional images without scanning. Those who are interested should refer to Ref. 8.

WAVEGUIDE EO DEVICES

Because a bulk EO device requires a device thickness equal to or greater than the beam diameter and a high S value, it is difficult to lower the applied voltage. If, however, we use an optical waveguide consisting of a core with a high refractive index and a cladding layer with a low refractive index, it is possible to confine most of the light within the core using the total reflection at the boundaries between the core and the cladding layers. This dramatically reduces the value of D/L, so making it possible to fabricate a compact low-voltage EO device.

The waveguide can be divided into slab waveguides and channel waveguides from the cross-sectional structure, as shown in Fig. 2. Channel waveguides include (b) the diffusion type, (c) ridged type, and (d) buried type. Figure 2(e) is another type of waveguide called ARROW with a leaky structure where light propagates with radiation of a small quantity of light into a substrate with a high refractive index (9). Dielectric materials including LN and $LiTaO_3$ crystals are diffusion type. Semiconductors such as GaAs and InP are ridged or buried type. Channel waveguides can be classified into several types shown in Fig. 3 where (a) is a linear waveguide, (b) is a curved waveguide, (c) is a tapered waveguide, (d) is the Y-branch, (e) is the X branch, and (f) is the directional coupler.

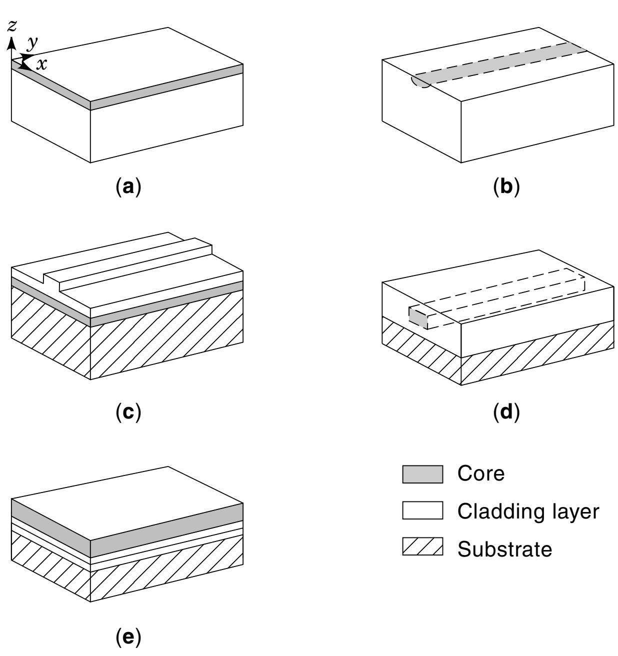

Figure 2. Various waveguide structures: (a) slab, (b) diffused, (c) ridged, (d) buried, (e) leaky structure.

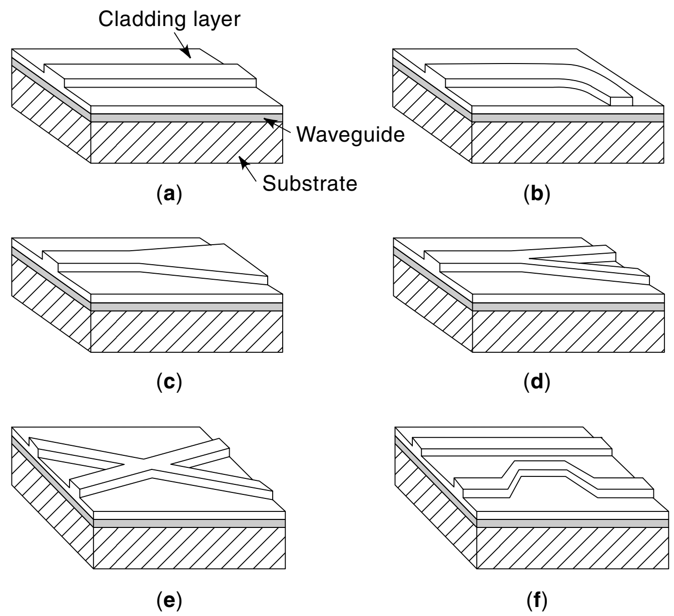

Figure 3. Various channel waveguide structures: (a) straight, (b) curved, (c) tapered, (d) Y branch, (e) X branch, (f) directional coupler.

The light propagating the slab waveguide in Fig. 2(a) is divided into two modes with different polarization states. One is the TE (transverse electric) mode possessing only the electric field component E_x in the x-axis direction and the magnetic field components H_y and H_z in the y- and z-axis directions. The other is the TM (transverse magnetic) mode possessing only the components H_x, E_y, and E_z. In channel waveguides, in which the refractive index difference between the core and its surrounding cladding layer is very small, light propagates while penetrating into the cladding layer. The guided beam therefore becomes a hybrid mode in which TE and TM modes coexist. For convenience, the light with E_x as its main component is called the TE-like mode, or simply TE mode. Similarly, light having E_y as its main component is called the TM-like mode or simply TM mode.

TE and TM modes are also called by such names as single mode or zeroth order mode, first-order mode, second-order mode, and so on, depending on the electric field distribution within the waveguide. Single mode is a guided beam without a node where the electric field intensity becomes 0 within the waveguide. Because single mode is stable and easy to control electrically, it is used in most EO devices. Nth mode ($N > 1$) is a guided beam with N nodes within the waveguide and is generally called multimode.

OPTICAL PHASE MODULATORS USING A CHANNEL WAVEGUIDE

Optical phase modulators have the simplest structure in which planar electrodes are loaded by a single-mode waveguide. Figure 4 shows a phase modulator using an LN crystal in which single-mode waveguide is formed on the surface of the crystal by thermal diffusion of Ti. When voltage V is applied to the planar electrodes with a gap D, the refractive indices of the waveguide in the z- and y-axes directions change according to Eq. (6). However, because the electrode has a planar structure, the refractive index change is different from that of the bulk modulator. If TE mode light is incident on the waveguide as shown in Fig. 4, the beam senses the refractive index change δ_n;

$$\delta_n = \xi n_e^3 r_{33} V/2D \tag{10}$$

where ξ is a coefficient indicating the overlap between the electric field distribution E_o of light and the applied electric field distribution E_a. When the applied electric field $E_a(y, z)$ in the y–z plane of the waveguide is expressed by $E_a(y, z) = e_a(y, z)V/D$, ξ is obtained by the following equation:

$$\xi = [\iint E_a(y,z) E_o^2(y,z)\,dy\,dz]/[\iint E_o^2(y,z)\,dy\,dz] \tag{11}$$

In the planar electrode structure, $E_a(y, z)$ is concentrated on the electrode's edge and decreases exponentially in the direction of depth. $E_o(y, z)$ becomes maximum at a location slightly apart from the waveguide surface. This means that in all waveguide devices not restricted to phase modulators, the overlap of the applied electric field and optical field is smaller than that of bulk optical modulators, and hence, $\xi < 1$. $E_a(x, y)$ can be determined using the finite element method (10) or successive overrelaxation method (11), and $E_o(x, y)$ can be determined by the effective index method (12) or Marcatili's method (13). In optical waveguides, a guided beam senses the effective index of refraction of the waveguide. The change δ_{en} of effective index of refraction is related to δ_n and expressed as

$$\delta_{en} = \zeta \delta_n \tag{12}$$

The product of ξ and ζ is called the reduction factor of an applied electric field, and this is normally expressed as Γ.

MACH–ZEHNDER TYPE OPTICAL MODULATOR

The Mach–Zehnder (M–Z) type optical modulator shown in Fig. 5 is one of the most well-known waveguide optical modulators. It is comprised of two phase modulators and two Y branches. This device's operation is easily understood from the mode selection function of the Y branch on the output

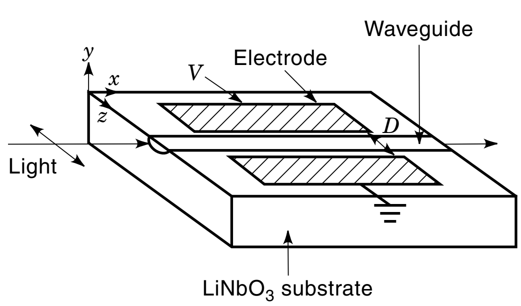

Figure 4. Basic structure of electooptic phase modulator.

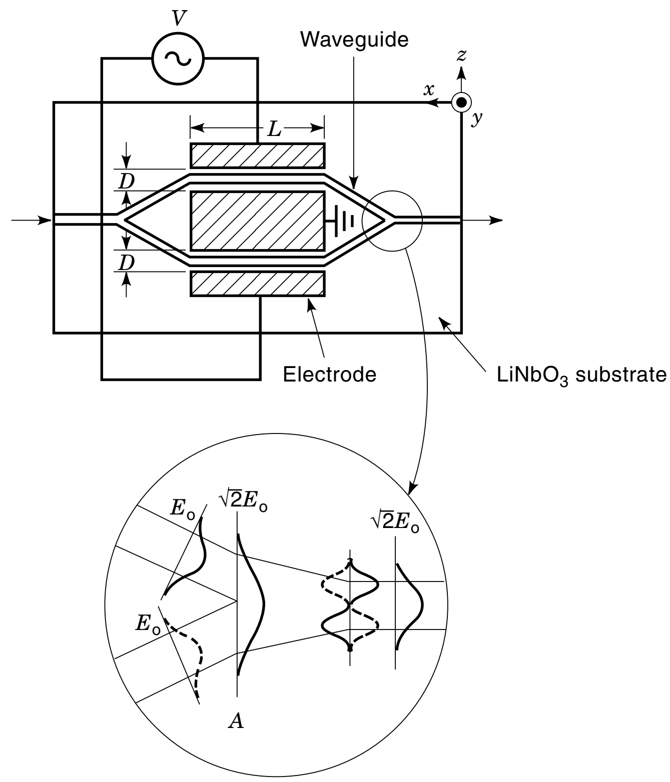

Figure 5. Top view of a Mach–Zehnder type optical modulator, which consists of two Y-branching waveguides and phase shifters. The circular figure shows the operating principle of the Y-branching waveguide. When two zero-order modes propagating in the Y branches are in-phase, even and odd modes are generated in order to satisfy the boundary condition at a point A. Two odd modes, which are of opposite phase, cancel each other out, and only even modes propagate through the output waveguide.

side. Now, let's discuss the operating principles for this device.

Consider the case where two single modes being in-phase propagate onto two single mode waveguides of the Y branch, as shown in the circle of Fig. 5. When the fundamental mode propagates in the upper waveguide and enters the tapered region, the even-mode, whose electric field distribution is symmetrically even, and the odd mode with odd symmetry are generated in order to satisfy the boundary condition at point A. Similarly, even and odd modes are generated when single-mode light propagating the lower waveguide enters the tapered section. Because the two odd-mode lights are in the opposite phase, they cancel each other out, resulting in only the even-mode lights of the same phase being output from the waveguide. This is the on state. Next, when both guided beams are in opposite phase, the guided beams are combined to transform into the first-order mode in the tapered region. Because this higher-order mode light cannot propagate in the single-mode waveguide, however, it is radiated into the substrate. This is the off state.

On the input-side Y branch, fundamental mode light propagating an input-side single-mode waveguide is divided into two single-mode lights with equal amplitude at the tapered section. In order to transfer the input single-mode light to two single-mode lights with minimum radiation loss at the branching point, the setting of branching angle ϕ is extremely important. If ϕ is too large, some of the light will be radiated into the substrate at the point of intersection. Usually, ϕ is around 1° with a considerable amount of radiation loss at the branching point. The radiation loss can be reduced as ϕ becomes small. It is noted, however, that the Y branch acts as the mode splitter of the lower-order and higher-order modes when ϕ is smaller than 1/100 rad.

When no voltage is applied to the electrodes on the M–Z type modulator, the single-mode lights propagating in both single-mode waveguides are in-phase, which means all the optical power is output (on state). Conversely, when voltage of the opposite polarity is applied to each electrode, the two guided beams passing through the electrode sections obtain phase changes. When the modulator is made from a Y-cut LN crystal, as shown in Fig. 5, the optical phase changes $+\theta$ and $-\theta$ in the upper and the lower waveguides, vice versa, and are expressed by Eq. (13), considering the push-pull operation of the modulator of interest:

$$\pm\theta = \pm\Gamma\pi n_e^3 r_{33} VL/\lambda D \tag{13}$$

where L is the electrode length and D is the electrode gap. When $\theta = \pi/2$, the phase difference between the two guided beams becomes π radian, the guided beams are transformed into the first-order mode and are radiated into the substrate (off state). The applied voltage required for this is known as the half-wave voltage V_π.

In order to apply this device to optical fiber communications, TE and TM modes must have the same phase change. Fortunately, because the relationship $n_e^3 r_{33} \fallingdotseq 3n_o^3 r_{13}$ forms for LN crystals, it is possible to set the phase changes of the TE and TM mode lights to around π and 3π by applying a voltage of $3V_\pi$ or lengthening the electrodes by a factor 3. Several kinds of polarization-independent M–Z type modulator have been manufactured using this relation. Furthermore, if we use a configuration in which light propagates along the z-axis direction and voltage is applied in the y-axis direction, we obtain analog optical modulators using the EO coefficient r_{22}, which produces optical phase changes with different polarity but same magnitude in TE and TM modes for any applied voltage (14). However, because the low-frequency EO coefficient r_{22}^{T} differs greatly from high-frequency EO coefficient r_{22}^{S} in magnitude, broadband modulation is difficult. In addition, because $r_{22}^{\mathrm{S}} \ll r_{33}^{\mathrm{T}}$, a high applied voltage is required.

Research on traveling-wave type devices in which microwave signals are supplied along the same direction as the light propagation direction is a current topic of interest. In these devices, the velocity matching of guided beams and microwave signals is crucial. Because the refractive indices of infrared light and microwaves are different, the thickness and shape of the electrode and the thickness of the buffer layer inserted between the electrode and waveguide are trimmed to reduce the effective refractive index of the microwaves and to expand the modulation bandwidth. Recently, an M–Z type LN waveguide modulator with a very wide bandwidth of over 100 GHz has been developed for application to optical fiber communication systems with a wider bandwidth than the direct modulation system using semiconductor lasers (15).

A unique feature of external modulation systems using optical waveguide modulators is their low- frequency chirping. There is also research on ways to control and use chirping. For example, there is a technique for expanding the transmission distance of a wavelength division multiplexing (WDM) system in which frequency chirping is generated in advance using an EO modulator consisting of an M–Z type modulator and a phase modulator on an LN crystal. In this system, frequency chirping generated in advance by the EO modulator compensates the waveform deterioration of optical pulses caused by an Er-doped fiber amplifier (16). Although the stability of LN waveguide devices has been greatly increased by improving the crystal quality and formation process for the buffer layer on waveguides, the problem of bias point fluctuation caused by dc drift has yet to be solved completely.

In the field of III-V compound semiconductors, extensive research is underway on M–Z type optical modulators with MQW structures. For example, M–Z type modulators using InGaAsP/InP has performed 15 GHz bandwidth modulation with a 10 dB extinction ratio and 2 V drive voltage (17). Research is also underway on the monolithic integration of optical amplifiers with M–Z type modulators (18). Compared to devices that use the Pockels effect, MQW structure devices have various superior features including a much shorter modulator and an extremely low drive voltage. Since the operating wavelength region is limited to near the bandgap, however, it is difficult to use in wavelength-multiplexing networks.

ELECTROABSORPTION MODULATOR

Because the EO effect of compound semiconductors is small compared to that of LN crystals, the mainstream of semiconductor modulators are the electroabsorption type using such phenomena as the QCSE and the Franz–Keldysh effect, which use electric fields to control absorption edge wavelengths. In particular, MQW optical modulators are attracting a great deal of attention. These sandwich an MQW structure consisting of periodically stacked super-thin semiconductor films with two different bandgaps between a p-type and an n-type cladding layers. This device has a number of advantages over conventional semiconductor waveguide modulators with no quantum-well structure, including (1) a shorter device length, (2) smaller device capacity, (3) operation at higher speeds, and (4) a lower applied voltage. The QCSE confines excitons generated by electroabsorption within narrow wells of MQW with a single-layer thickness of several nanometers and then adds an electric field to perform modulation by shifting the absorption peak to the long wavelength side. To hold excitons for a long period, a bulk crystal must be kept at a low temperature, but because the binding energy in the quantum well structures is large, here excitons exist stably even at room temperature.

Figure 6 shows an MQW optical modulator (19). The InGaAs/InAlAs layer with 12 wells is an electroabsorption layer, and an electric field is applied through the p-InAlAs and n-InAlAs layers. Because the modulator length (63 μm) is too short for cleaving, passive regions with an InGaAs/InP waveguide are attached on either end of the modulator. This device boasts superior performance: a 3 dB bandwidth of 50 GHz, a drive voltage of 2.8 V, and an extinction ratio of 20 dB, except for an insertion loss of 8 dB.

The monolithic integration of MQW optical modulators and DFB (distributed feedback) lasers is also flourishing. For ex-

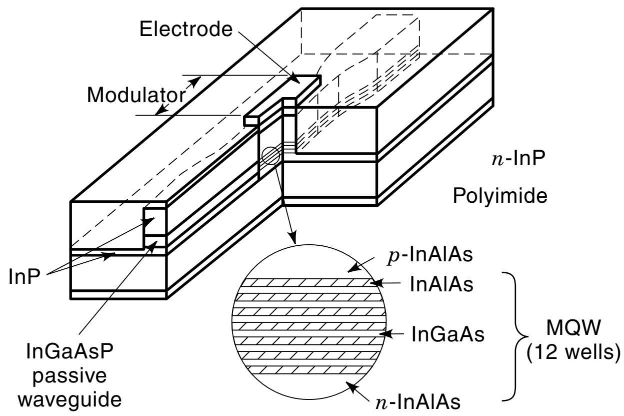

Figure 6. Schematic configuration of an electroabsorption modulator. The electroabsorption effect based on the QCSE is so large that this modulator is far shorter than the waveguide modulator using the Pockels effect.

ample, NRZ (nonreturn-to-zero) operation at 40 Gb/s has been performed using an MQW electroabsorption modulator integrated with a DFB laser driven by dc current (20). Five MQW optical modulators have been integrated on an InP substrate and a multiplexing of 100 Gb/s optical pulses has been achieved using them (21). In addition to these experiments, a blue-chirping MQW optical modulator using an InGaAlAs/InAlAs MQW layer about 20 nm thick has also been reported. This device has a negative α parameter, which expresses the magnitude of chirping, due to the quantum-confined Franz–Keldysh effect, and is therefore suited to long-distance transmissions (22). The electroabsorption modulators have advantages over LN modulators in the point of monolithic integration with light emitting devices and photodetectors. They also have several problems, such as large optical insertion loss, including coupling loss caused by connecting with an optical fiber, propagation loss, and an insufficient extinction ratio. Practical application will therefore likely come after the LN waveguide devices.

DIRECTIONAL COUPLERS

Devices in which two parallel single-mode waveguides whose propagation constants are identical or very close to each other are so close together that the tails of the guided modes overlap are known as directional couplers. The two waveguides are considered to be a couple of waveguides in which the odd and even modes propagate. Because the odd mode and even mode propagation constants β_o and β_e are just slightly different, a beat of both modes is generated, enabling the transfer of power between the two waveguides.

We discuss a case in which a single-mode light flows in the waveguide 1 at the same propagation constant as that of waveguide 2, as shown in Fig. 7 where Ti-diffused single-mode waveguides are formed on a Z-cut LN crystal. We first assume that no electrode is deposited on this device. In waveguide 1, at a point where $z = 0$, the generated odd mode and even mode are in phase, and in waveguide 2 both modes are in opposite phase to each other. At a point where $z = L$, both modes are in opposite phase in waveguide 1 and in-phase in waveguide 2 due to the difference of the propagation constants, as shown in Fig. 7. That is, all power of light flowing in waveguide 1 transfers to waveguide 2 at the point where $z = L$. We call L the coupling length. This is one of the important parameters of the directional coupler. When distance z exceeds L, power returns to waveguide 1 and the transfer of optical power repeats cyclically according to propagation distance z. If we expand the waveguide distance at the position where $z = L$, as shown in Fig. 7, we can extract all the power of the light from waveguide 2.

According to the coupled-mode theory (23), the normalized output intensities P_1 and P_2 from waveguides 1 and 2 are expressed as follows:

$$\begin{aligned} P_1 &= \cos^2(\kappa z) \\ P_2 &= \sin^2(\kappa z) \end{aligned} \tag{14}$$

where κ is the coupling coefficient related to the coupling length and depends on such factors as the propagation constant, the distance between waveguides, and the waveguide width.

We can build an optical modulator/switch by loading planar electrodes to a directional coupler and electrically changing the propagation constant of the two waveguides. When electrically induced, difference of the propagation coefficients is expressed as $\Delta\beta$; the outputs P_1 and P_2 of the two waveguides can be given by the following equations (24):

$$\begin{aligned} P_1 &= \cos^2(gz) + (\Delta\beta/2g)^2 \sin^2(gz) \\ P_2 &= (\kappa/g)^2 \sin^2(gz) \\ g^2 &= \kappa^2 + (\Delta\beta/2)^2 \end{aligned} \tag{15}$$

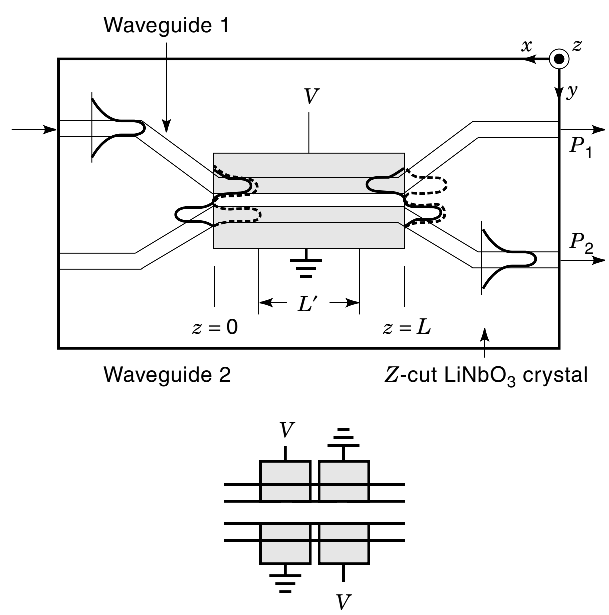

Figure 7. Top view of the directional coupler. All optical power of the beam propagated in waveguide 1 is transferred to waveguide 2 after passing through the mode-coupling zone of a coupling length L. The power transfer can be controlled by changing the refractive indices of the waveguides. The lower figure shows the stepped $\Delta\beta$ reversal type electrode structure, which easily obtains the maximum extinction ratio and minimum crosstalk.

When the applied voltage is zero, the condition in which $P_1 = 0$ and $P_2 = 1$ at $z = L$ is $\kappa L = (m + \frac{1}{2})\pi$ $(m = 0, 1, 2, \ldots)$. When voltage is applied, the condition in which $P_1 = 1$, $P_2 = 0$ is $gL = (m + 1)\pi$. Under these conditions, the half-wave voltage required for a 100% power transfer is as follows:

$$V_\pi = \sqrt{3}D\lambda/(2\Gamma n_e^3 r_{33} L) \tag{16}$$

where we assumes that the electrode length is L and the gap between the electrodes is D.

The device in Fig. 7 can transfer 100% of the optical power only when $kL = (m + \frac{1}{2})\pi$. In order to improve this, a reversed $\Delta\beta$ directional coupler (25) has been proposed. It has two pairs of planar electrodes of the same length, as shown in the small figure in Fig. 7. This configuration has achieved, for the first time, a directional coupler with a high extinction ratio and has been applied to matrix switches.

OPTICAL WAVEGUIDE SWITCHES

There are two kinds of switches. One is the optical waveguide switch, which changes the ports outputting the guided beams one dimensionally, and the other is the two-dimensional optical switch, which changes light beams spatially. Waveguide optical switches include the balanced bridge type in Fig. 8(a), the total reflection type in Fig. 8(b), the Y-branch type in Fig. 8(c) and the asymmetric X-branch type in Fig. 8(d), in addition to the previously mentioned directional coupler. The advantages of the balanced bridge type are its low drive voltage and the large design tolerance because it is comprised of a 3 dB coupler and a phase shifter. Because the device is long, it is suited to small matrix switches.

The total reflection type employs total internal reflection at the X-crossing portion. At first, optical switches using LN crystals were proposed, but they had a number of problems including too much crosstalk and the need for high drive voltages. Recently, a carrier injection type semiconductor optical switch made up of an X-crossing waveguide and Y-branching switches has been proposed. A prototype 4 × 4 matrix switch integrating this device on an InP substrate has been manufactured (26). It has also been demonstrated that the optical insertion loss can be adequately compensated for by integrating the optical switch and an optical amplifier.

The Y-branch type uses the refractive index change in the branch portion to switch optical paths. Like the total reflection type, 1 × 2 and 1 × 4 Y-branch type switches using LN crystals were fabricated earlier than the semiconductor switches (27). These devices have the advantage of shorter device length than directional couplers but need a relatively high voltage to operate with low crosstalk. Semiconductor devices employ phenomena such as QCSE to enable a large change in the refractive index at low voltages. Based on this, research is underway on 1 × 2, 4 × 4, and other switches. The optical output versus applied voltage properties of the previously mentioned total reflection type and Y-branch type do not have a repetitive nature so they are suitable for digital operation. If a bipolar voltage with sufficient amplitude is applied, it is possible simultaneously to switch TE and TM modes. An InGaAsP/InP 4 × 4 matrix switch has been reported having properties such as a 2.5 GHz modulation bandwidth, 15 dB crosstalk, 5 dB insertion loss, and 4.5 V switching voltage (28).

The asymmetric X-waveguide type has a structure combining a symmetric Y branch consisting of single-mode waveguides ①, ② with an equal width and asymmetric Y branch consisting of a wide waveguide ③ and a narrow waveguide ④. In an asymmetric Y branch, the fundamental mode of the combined portion flows to the wide waveguide with a large

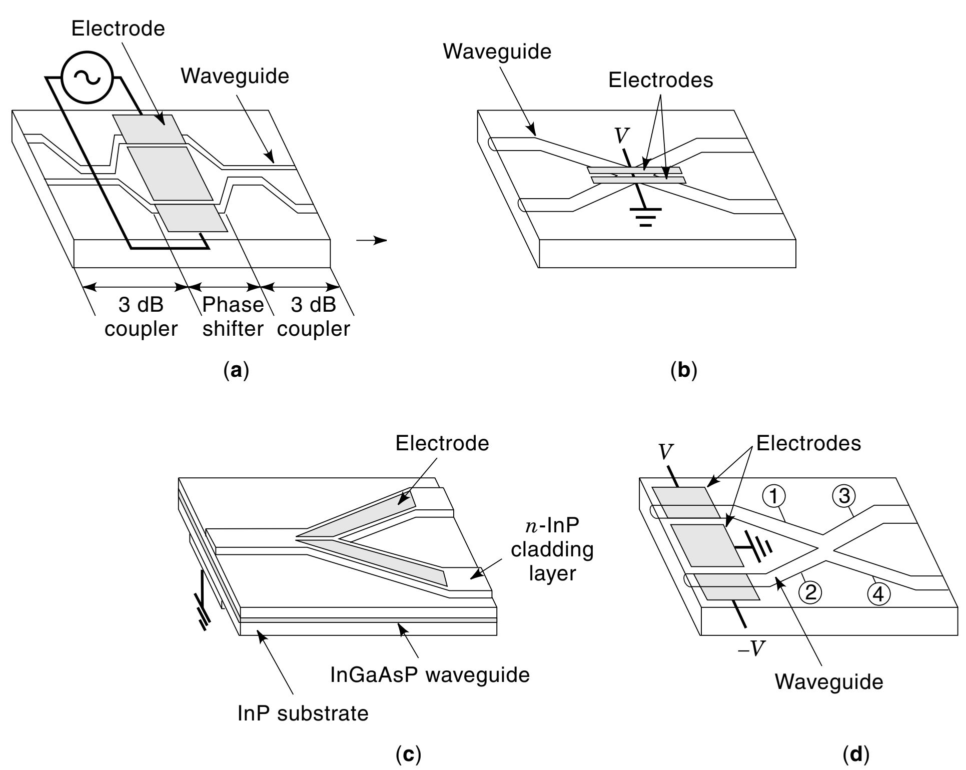

Figure 8. Various waveguide switches: (a) balanced bridge, (b) total reflection, (c) Y branch, (d) asymmetric X branch.

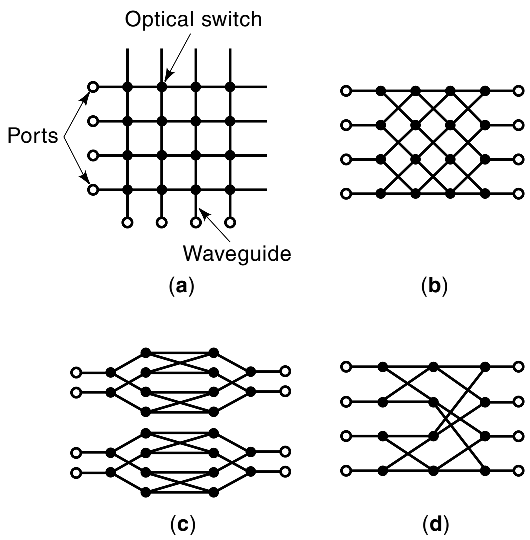

Figure 9. Various matrix switch structures. The cross point and linear line are an optical switch and a channel waveguide, respectively: (a) crossbar, (b) square arrangement, (c) tree, (d) simplified tree.

effective refractive index, whereas the high-order mode flows to the narrow waveguide. Consequently, when two single-mode in-phase beams travel from the Y branch to the asymmetric Y branch, both guided beams passing through the combined portion are focused completely on the wide waveguide. When the two guided beams are in opposite phase, the beams converge on the narrow waveguide. The asymmetric X waveguide type can be used to build a compact Michelson interferometer, so sensing devices using LN crystals have been explored.

Matrix switches integrating these optical waveguide switches are the primary devices in optical fiber communications and photonic switching systems, and development in this area is progressing vigorously. The first matrix switch to be proposed was the crossbar type shown in Fig. 9(a). Because this architecture is problematic in terms of the many crosspoints through which the guided beams pass and the fluctuation of their number owing to the connection state, it has been difficult to increase the number of ports. Configurations such as the square arrangement type shown in Fig. 9(b), tree type shown in Fig. 9(c) and simplified tree type shown in Fig. 9(d) have been proposed to rectify the problem. Because the simplified tree type has the fewest crosspoints as well as low crosstalk, various kinds of matrix switches have been produced using this type as the basic configuration. For example, a 16×16 matrix switch was achieved using LN directional couplers (29). This device was 70 mm long and had 56 switches, 2 mm long electrodes, a 10 V drive voltage, and 25 dB crosstalk. To enlarge the matrix size over the previously mentioned device is probably difficult because of the LN crystal size. Development is also underway on a polarization-independent matrix switch that can simultaneously switch TE and TM modes, and prototype 8×8 devices using an LN crystal have been produced (30).

In the area of semiconductors, a prototype of an 8×8 matrix switch has been produced consisting of GaAs/AlGaAs directional coupler switches using the EO effect. This prototype was 26.5 mm long and had 56 switches, an 8.7 dB insertion loss, a 25 V drive voltage, and 21 dB crosstalk (31). Because most matrix switches using effects other than the EO effects such as QCSE and carrier injection have low drive voltages but high insertion loss, manufactured prototypes have gone no farther than devices with 4×4 or fewer. It is apparent at the present time that there is a low degree of integration in matrix switches using semiconductors. However, because they have excellent features such as ease of size-reduction and the capability for integrating optical amplifiers, they have a brighter looking future than LN crystals.

TWO-DIMENSIONAL OPTICAL SWITCHES

Two-dimensional optical switches are intended for applications such as optical interconnections, which use light to perform signal connection in parallel between boards containing processors and between racks of multiple boards, and optical computing, which uses light to process images and two-dimensional bit patterns simultaneously. Because parallel connections of at least 1000 ports are demanded from two-dimensional optical switches, surface normal switches that can send and receive optical signals to a substrate perpendicularly are considered suitable. Surface normal switches are classified either as the nonradiative type, integrating optical modulators, or the radiative type, integrating such devices as semiconductor lasers and photodetectors.

Well-known examples of nonradiative devices include the GaAs Fabry–Perot etalon and SEED. A number of structures for the GaAs Fabry–Perot etalon have been proposed. First, a device sandwiching GaAs/AlGaAs MQW layers with GaAs/AlGaAs multilayer film reflectors was proposed, but recently there has been a proposal for a *p-i-n* photodiode having an MQW layer and multilayer film reflectors with different reflectivity. This device has achieved a modulation efficiency of 20%, extinction ratio of 15, and pulse response time of 130 ps (32). The structure of FP devices is simple, but because they possess a resonator structure, their problems include low design tolerance for device thickness and bias voltage and susceptibility to temperature changes.

A SEED has an MQW layer in which the superlattice structure consisting of GaAs layers and GaAlAs layers is formed in part of the *i* layer of a *p–i–n* photodiode (33). In this device, a feedback circuit is formed by connecting a resistor, photodiode, phototransistor, FET, and other elements to this *p–i–n* photodiode. The device known as the resistor-biased SEED (R-SEED), which connects a resistor [Fig. 10(a)], was the first to be developed. Let's take the R-SEED as an example and discuss how it operates. Irradiating light of a wavelength near the exciton absorption edge to the MQW layer results in a low photocurrent when the light power P_{in} is low and most of the bias voltage is applied to the photodiode. Because of the QCSE, the absorption edge moves to the long wavelength side, resulting in low light absorption. In this case, the output light power P_{out} is small. Increasing the light power causes the photocurrent to increase and the electric field applied to the diode though external resistor R to decrease. Because the absorption edge returns to the short wavelength at that time, light absorption increases, as does the photocurrent. Because of this positive feedback effect, input light power P_{in} vs. output light power P_{out} characteristics of the SEED show bistability.

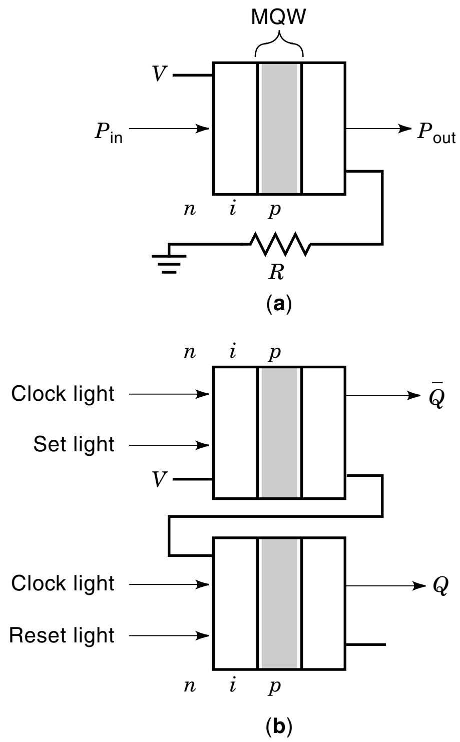

Figure 10. Basic configuration of SEED. In (a), R-SEED consists of a *p-i-n* photodiode with an MQW light absorption layer and a resistor and shows optical bistability. Exchanging the resistor for the same *p-i-n* photodiode with an MQW light absorption layer, the S-SEED shown in (b) can be obtained. Many kinds of digital optical systems aiming at optical interconnection and optical processing have been investigated using S-SEEDs.

The device consisting of two SEEDs connected in series and forming a feedback circuit, as shown in Fig. 10(b), is known as a symmetric SEED (S-SEED) (33). Exposing the two SEEDs to a set pulse light and a reset pulse light with low-luminance causes this device to perform a flip-flop operation. In addition to these pulses, when high-luminance clock pulse lights, which are one pulse width behind the set and reset pulses, are applied to S-SEEDs, output light Q and $\overline{Q}$ obtain a time-sequential gain, enabling switching with a superior SNR. The integration of this device has reached 8K (128 × 64) and 32K (256 × 128) (34). Development is also underway on a free-space optical switching network that performs multistage switching of integrated S-SEEDs. Recent experiments demonstrated the interconnection of two 32 × 16 S-SEED arrays (35).

In addition to these developments, work is also underway on integrating GaAs-FETs and Si-CMOS transistors with S-SEEDs, and research on smart pixels that possess optical signal distribution and electronic circuit signal processing functions is flourishing (36). SEEDs must integrate a large number of elements to handle images, but they do have a number of strong points including (1) operation at low light energy, (2) a fast response (the speed is inversely proportional to light energy), and (3) superior compatibility with integrated circuits.

The radiative-type surface normal switches that we know of are vertical-cavity surface-emitting lasers (VCSEL), devices combining FETs with photodiodes, and vertical to surface transmission electrophotonic devices (VSTEP) that have a *pnpn* structure. VSTEPs are AlGaAs surface normal photoemitters formed on a GaAs substrate. They have a variety of functions, including photodetection, photoemission, switching, optical amplification, and memory. The optical emission function has an LED mode as well as a laser mode by means of a device provided with multilayer mirrors on the top and bottom of the device. Up to the present, a two-dimensional array (32 × 32) with functions, such as optical switching and optical latching using VSTEPs has been reported, and tests are underway on optical connections using electric and optic signals (37).

Radiative-type integrated devices have advantages such as high on/off and gain, and problems of high power consumption and accumulation of heat during parallel operation. Even nonradiative type devices require a light source for emitting light; however, radiative-type devices will probably be beneficial to future large-scale optical interconnections and optical computing.

BIBLIOGRAPHY

1. R. G. Hunsperger, *Integrated Optics: Theory and Technology,* Berlin: Springer-Verlag, 1984, 2nd ed., pp. 144–157.
2. B. Bahadur (ed.), *Liquid Crystals: Applications and Uses,* Singapore: World Scientific, 1990, vols. 1–3.
3. S. E. Miller, Integrated optics: An introduction, *Bell Syst. Tech. J.,* **48**: 2059–2069, 1969.
4. R. V. Schmit and I. P. Kaminow, Metal-diffused optical waveguides in $LiNbO_3$ and $LiTaO_3$, *Appl. Phys. Lett.,* **25**: 458–460, 1974.
5. K. Takizawa and M. Okada, Determination of relative signs of electro-optic and piezoelectric coefficients by measuring optical phase shifts caused by an applied electric field, *J. Opt. Soc. Am. B,* **2**: 289–293, 1985.
6. I. P. Kaminow and E. H. Turner, Electrooptic light modulators, *Appl. Opt.,* **5**: 1612–1628, 1966.
7. K. Takizawa and M. Okada, Time-division power divider using electrooptic light switches, *J. Lightw. Technol.,* **LT-4**: 169–175, 1986.
8. S. H. Lee (ed.), *Optical Information Processing: Fundamentals,* New York: Springer-Verlag, 1981, pp. 121–126.
9. T. Baba and Y. Kokubun, Dispersion and radiation loss characteristics of antiresonant reflecting optical waveguide-numerical results and analytical expressions, *IEEE J. Quantum Electron.,* **28**: 1689–1700, 1992.
10. O. C. Zienkiewicz and Y. K. Cheung, *The Finite Element Method in Engineering Science,* New York: McGraw-Hill, 1971.
11. H. E. Green, The numerical solution of some important transmission-line problems, *IEEE Trans. Microw. Theory Tech.,* **MTT-13**: 676–692, 1965.
12. T. Tamir, *Integrated Optics,* New York: Springer-Verlag, 1975, chap. 2.
13. E. A. J. Marcatili, Dielectric rectangular waveguide and directional coupler for integrated optics, *Bell Syst. Tech. J.,* **48**: 2071–2102, 1969.
14. K. Takizawa, M. Okada, and T. Aida, Polarization-independent and optical-damage-insensitive $LiNbO_3$ interferometric waveguide modulator, *Jpn. J. Appl. Phys.,* **27**: L696–L698, 1988.
15. K. Noguchi, O. Mitomi, and H. Miyazawa, Low-voltage and broadband Ti:$LiNbO_3$ modulators operating in the millimeter wavelength region, *OFC Tech. Dig.,* 1996, pp. 205–206.

16. M. Seino, LN-waveguide devices for high-speed or WDM systems, *Meet. Electron. Soc. Inst. Electron., Inf. Commun. Eng. Jpn.,* 1997, pp. 361–362.
17. C. Rolland et al., 10 Gbit/s, 1.56 μm multiquantum well InP/InGaAsP Mach-Zehnder optical modulator, *Electron. Lett.,* **29**: 471–472, 1993.
18. J. E. Zucker et al., Interferometric quantum well modulators with gain, *IEEE J. Lightw. Technol.,* **10**: 924–932, 1992.
19. T. Ido et al., Ultra-high-speed multiple-quantum-well electro-absorption optical modulators with integrated waveguides, *IEEE J. Lightw. Technol.,* **14**: 2026–2034, 1996.
20. H. Takeuchi et al., NRZ operation at 40 Gb/s of a compact module containing an MQW electroabsorption modulator integrated with a DFB laser, *IEEE J. Photon. Technol. Lett.,* **9**: 572–574, 1997.
21. F. Zamkotsian et al., Monolithic integration of MQW modulators on an optical multiplexer on InP for 100 Gb/s transmission, *IEEE J. Lightw. Technol.,* **14**: 2344–2352, 1996.
22. K. Wakita et al., Blue-chirp electroabsorption modulators with very thick quantum wells, *IEEE Photon. Technol. Lett.,* **8**: 1169–1171, 1996.
23. E. A. J. Marcatili, *Bell Syst. Tech. J.,* **48**: 66–73, 1969.
24. R. G. Hunsperger, *Integrated Optics: Theory and Technology,* Berlin: Springer-Verlag, 1984, pp. 129–132.
25. H. Kogelnik and R. V. Schmidt, Switched directional couplers with alternating $\Delta\beta$, *IEEE J. Quantum Electron.,* **QE-12**: 396–401, 1976.
26. H. Inoue et al., An 8 mm length nonblocking 4×4 optical switch array, *IEEE J. Sel. Areas Commun.,* **SAC-6**: 1262–1266, 1988.
27. M. Haruna and J. Koyama, Electrooptical branching waveguide switches and the application to 1×4 optical switching network, *IEEE J. Lightw. Technol.,* **LT-1**: 223–227, 1983.
28. M. Renaud, M. Bachmann, and M. Erman, Semiconductor optical space switches, *IEEE J. Sel. Top. Quantum Electron.,* **2**: 277–288, 1996.
29. P. J. Duthie, M. J. Wale, and I. Bennion, Size, transparency and control in optical space switch fabrics: 16×16 single chip array in lithium niobate and its applications, *Top. Meet. Photon. Switch.,* Kobe, 1990, pp. 13a-3.
30. S. Suzuki et al., *Tech. Dig. Top. Meet. Photon. Switch.,* Salt Lake City, UT, 1991, p. FE1.
31. K. Hamamoto et al., First 8×8 semiconductor optical matrix switches using GaAs/GaAlAs directional couplers, *Electron. Lett.,* **28**: 441–443, 1992.
32. R. H. Yan, R. J. Simes, and L. A. Coldren, Analysis and design of surface-normal Fabry-Perot electrooptic modulators, *IEEE J. Quantum Electron.,* **25**: 2272–2280, 1989.
33. D. A. B. Miller, Quantum-well self-electro-optic effect devices, *Opt. Quantum Electron.,* **22**: S61–S98, 1990.
34. L. M. F. Chirovsky et al., *Photon. Switch. Top. Meet.,* Salt Lake City, UT, 1991, p. ThB3.
35. F. B. McCormick et al., Experimental investigation of a free-space optical switching network by using symmetric self-electro-optic-effect devices, *Appl. Opt.,* **31**: 5431–5446, 1992.
36. D. J. Goodwill, K. E. Devenport, and H. S. Hinton, An ATM-based intelligent optical backplane using CMOS-SEED smart pixel arrays and free-space optical interconnect modules, *IEEE J. Sel. Top. Quantum Electron.,* **2** (1): 85–96, 1996.
37. T. Numai et al., Surface-emitting laser operation in vertical-to-surface transmission electrophotonic devices with a vertical cavity, *Appl. Phys. Lett.,* **58**: 1250–1252, 1991.

KUNIHARU TAKIZAWA
Japan Broadcasting Corporation